Eigenvalue Matrix Analysis of Segmented Stripline Junction Disk Circulator

Kevin M. Gaukel, *Member, IEEE*, and El-Badawy El-Sharawy, *Senior Member, IEEE*

***Abstract*—An accurate and numerically efficient analysis technique for tightly coupled three-port stripline circulators is discussed. By using the three-way symmetry of the network, the port-only segmentation analysis is reduced to generating and solving three smaller "eigenvalue matrices." In addition, accuracy enhancement is shown by weighting the subport characteristic impedances and subport angles to more accurately reflect the current distribution of the ports.**

I. Introduction

ANALYSIS of three-port triplate stripline disk circulators has been performed in variations of constant current Green's Function analysis by Bosma [1]. More intricate numerical techniques such as the finite element method presented by Lyon and Helszajn [2] and the integral equation techniques presented by Okoshi [14] and Miyoshi *et al.* [3], [4] have also been presented. Bosma's approach is limited by its nonrealistic current distribution to coupling angles of less than 0.25 radians [5]. The integral equation technique, which segments the entire disk structure and discretely solves the Green's Function Equation at each segment, may not be easy to implement as an iterative design tool because of the large matrices required to generate solutions. Similarly, the finite element analysis requires a complex mesh generating algorithm as well as a large amount of computing capacity.

A numerical approach presented by the authors [6] reduced the matrix size by restricting the subdivision of the structure to the ports themselves. These segments are assumed to be directly connected just outside of the coupling ports. This analysis reduced the required impedance matrix size to $3N \times 3N$, where N is the number of subports within each port. Unlike the segmentation analysis presented by Okoshi [14], the port-only analysis utilized the segmentation only as a means to predict the current distribution across each port. Once the current density was determined, the ports were assumed connected, and the circulator is reduced to a three-port device. Since there were no interface networks other than the port connections, the number of matrix operations required were reduced.

The present analysis utilizes the cyclic symmetry of the circulator network to reduce the required matrix size to three $N \times N$ matrices made up of the eigenvalues of the cyclic submatrices. These eigenvalues matrices reduce to the "0," "+1," and "−1" admittance eigenvalues of the circulator being modeled. The present approach improves the numerical efficiency by a factor of 9.

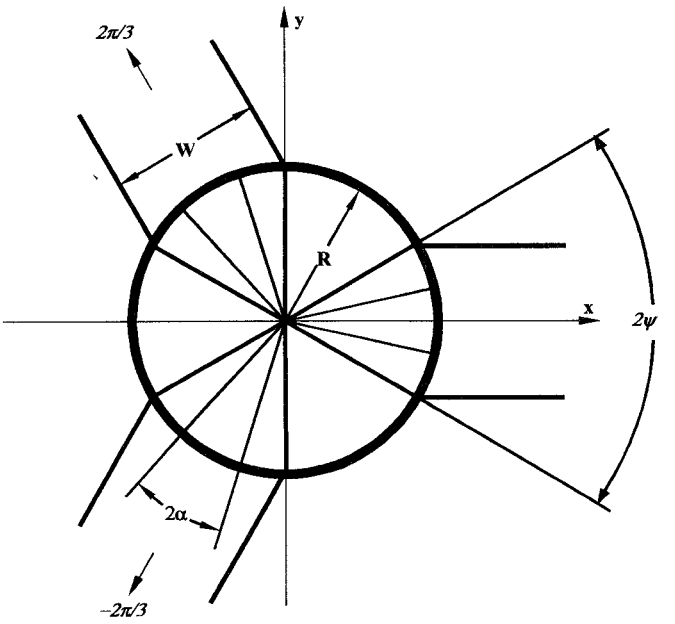

Fig. 1. Three-port disk circulator with subdivided ports.

Accuracy is also improved by weighting the subport stripline feed impedances to take into account the edge conditions of the stripline feeding the circulator. Since the voltage is assumed constant, the edge current distribution is more accurately represented by making the outer subports lower in impedance than the central subport. The resulting accuracy enhancement allows for use of much fewer subports and therefore much smaller matrices.

When the subport model is compared to experimental data on a three-port quarter-wave coupled circulator, the subport analysis is shown to be accurate in terms of impedance, bandwidth, and midband isolation. Weighting improves the accuracy even further, although more modes were required to accurately calculate the impedance matrix term.

II. Direct Calculation of Subport Matrix

The basic port-only analysis in [6] starts with a three-port disk resonator of radius R coupled with three stripline ports with coupling angle 2ψ as shown in Fig. 1. The stripline ports are segmented into N subports, each with coupling angle 2α. The resonator periphery not within the ports is assumed to have zero magnetic field, and the total port coupling angle is

Manuscript received June 20, 1994; revised December 16, 1994.

K. M. Gaukel is with Celwave, R.F., Phoenix, AZ USA.

E. El-Sharawy is with the College of Engineering and Applied Sciences, Arizona State University, Tempe, AZ 85287-7206 USA.

IEEE Log Number 9412032.

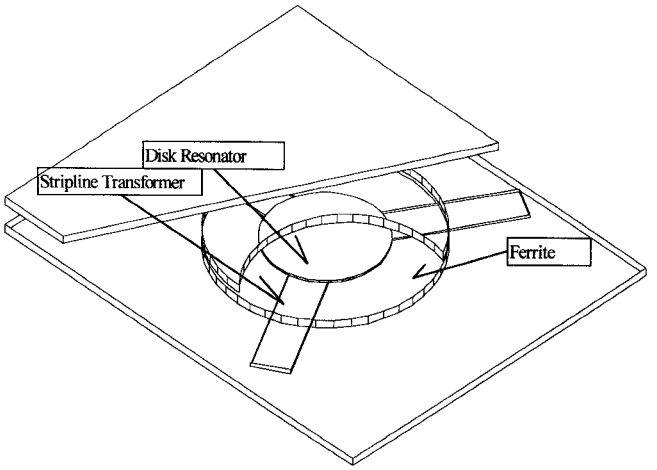

Fig. 2. Isometric view of stripline circulator being modeled.

$2N\alpha$. The physical width of the main port and the subport are given in (1) and (2) in terms of the coupling angles

$$w = 2R\sin(\psi) \tag{1}$$

$$w_\alpha = 2R\sin(\alpha). \tag{2}$$

The network in Fig. 1 is placed in between two ferrite substrates and two perfect electric conductor sheets to form a stripline configuration, as shown in Fig. 2. The region outside of the ferrite is air, and there are no other dielectrics in the structure. The ferrite has a dielectric constant of ϵ_f, and its permeability is determined as a tensor of the form given in (3)

$$\mu = \begin{bmatrix} \mu & -j\kappa & 0 \\ j\kappa & \mu & 0 \\ 0 & 0 & \mu_0 \end{bmatrix}. \tag{3}$$

The terms μ and κ are determined by the external DC-applied field and are well known in literature [1], [10]. From these, the effective permeability of a radially travelling wave in the ferrite is determined from μ and κ in (4)

$$\mu_{eff} = \frac{\mu^2 - \kappa^2}{\mu} \tag{4}$$

and the propagation constant of a TEM wave in the ferrite is given in (5) in terms of μ_{eff}, ϵ_f, and the frequency ω

$$\beta_e = \omega\sqrt{\mu_{eff}\epsilon_f}. \tag{5}$$

The impedance matrix for the structure in Fig. 1 was determined in [6] by assuming that the electric field was constant just beyond the disk edge and that only TEM modes propagated in the stripline. The result of the analysis is given in (6)

$$Z_{q_{st}r_{lm}} = jZ_e\psi \sum_{n=-\infty}^{\infty} \mathcal{R}_n(\alpha)e^{-jn(\varphi_{lm}-\varphi_{st})} \tag{6}$$

where the angle φ_{lm}, series prefix term $\mathcal{R}_n(\alpha)$, and matrix indices q and r are determined in (7)–(10)

$$\varphi_{lm} = \left(\frac{2m-1}{N} - 1\right)\psi + \frac{2\pi}{3}(l-1) \tag{7}$$

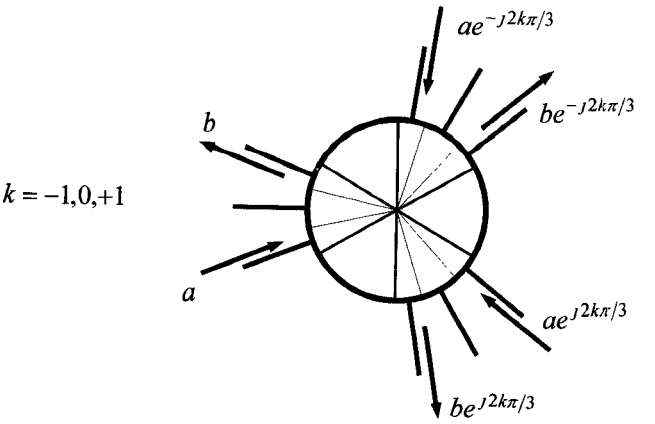

Fig. 3. Eigenvector excitation and detection of adjacent subports.

$$\mathcal{R}_n(\alpha) = \frac{\sin^2(n\alpha)}{(n\alpha)^2}\left[\frac{J_n'(\beta_e R)}{J_n(\beta_e R)} - \left|\frac{\kappa}{\mu}\right|\frac{n}{\beta_e R}\right]^{-1} \tag{8}$$

$$q_{st} = t + N(s-1) \quad s = 1, 2, 3 \quad t = 1, 2, \cdots, N \tag{9}$$

$$r_{lm} = m + N(l-1) \quad l = 1, 2, 3 \quad m = 1, 2, \cdots, N. \tag{10}$$

The quantity Z_e given in (6) is the subport stripline feed impedance given approximately in equation (11) for the triplate stripline whose width is much greater than height [8].

$$Z_e \approx 30\pi\sqrt{\frac{\mu_{eff}}{\epsilon_f}}\frac{h}{w}. \tag{11}$$

III. Eigenvalue Matrix Approach

The matrix, whose elements are expressed in (6), is much smaller in size than the integral equation method described by Okoshi and Miyoshi [14] for a given port resolution. However, the present matrix has many extraneous elements that add unnecessary calculations to the analysis. To demonstrate this, the subport impedance matrix is written in the following form:

$$\mathbf{Z}'_{tm} = \begin{bmatrix} \{\mathbf{Z}_{11}\}_{tm} & \{\mathbf{Z}_{12}\}_{tm} & \{\mathbf{Z}_{13}\}_{tm} \\ \{\mathbf{Z}_{13}\}_{tm} & \{\mathbf{Z}_{11}\}_{tm} & \{\mathbf{Z}_{12}\}_{tm} \\ \{\mathbf{Z}_{12}\}_{tm} & \{\mathbf{Z}_{13}\}_{tm} & \{\mathbf{Z}_{11}\}_{tm} \end{bmatrix} \tag{12}$$

where $\{\mathbf{Z}_{sl}\}$ is a submatrix corresponding to output port s and input port l. The tm element of the submatrix is determined in (13)

$$\{\mathbf{Z}_{sl}\}_{tm} = jZ_e\psi \sum_{n=-\infty}^{\infty} [\mathcal{R}_n(\alpha)e^{jn(t-m)\alpha}][e^{j2\pi/3}]^{n(s-l)}. \tag{13}$$

The phase term $e^{j2\pi/3}$ occurs in (13) because there is a correspondence between a given input and any three subports that have 120-degree angular separation. If, for example, we divide each port into three subports, as shown in Fig. 3, the phase relation between subports 1, 4, and 7 are exactly the same as 2, 5, and 8 as well as 3, 6, and 9. This is referred to in literature as cyclic symmetry [8].

Riblet has demonstrated in the case of the integral equation technique that the symmetry allows the impedance matrix to be reduced to a series of eigenvalue matrices [13]. In a

TABLE I
NUMBER OF OPERATIONS TO INVERT SUBPORT MATRIX

Number of Subports	Number of Multiplications using Direct Analysis	Number of Additions using Direct Analysis	Number of Multiplications using Eigenvalue Matrix	Number of Additions using Eigenvalue Matrix
2	216	150	24	6
3	729	576	81	36
5	3375	2940	375	240
7	9261	8400	1029	756
9	19683	18252	2187	1728

similar manner, the subport impedance matrix in (12) has the same cyclic symmetry, so we can write (12) in terms of three eigenvalue matrices $\mathbf{Z}_0$, $\mathbf{Z}_{+1}$, $\mathbf{Z}_{-1}$. Each eigenvalue matrix $\mathbf{Z}_k$ can be written in terms of the submatrices in (12), as shown in the following equation:

$$\{\mathbf{Z}_k\} = \{\mathbf{Z}_{11}\} + e^{-j2k\pi/3}\{\mathbf{Z}_{12}\} + e^{j2k\pi/3}\{\mathbf{Z}_{13}\}. \quad (14)$$

Substituting (13) into (14) results in the following equation for each element in $\mathbf{Z}_k$:

$$\{\mathbf{Z}_k\}_{tm} = j3Z_e\psi \sum_{v=-\infty}^{\infty} \mathcal{R}_{3v-k}(\alpha)e^{-j2(3v-k)(m-t)\alpha} \quad (15)$$

where v is summation index of the eigenvalue matrix element. The change in indices occurs because the 120-degree phasing terms cancel for all terms except when $n + k$ is a multiple of three, where n is the index of the summation in (13) and k is the eigenvalue index.

The main reason for expressing the eigenvalue matrix elements as a summation is that the analysis of the three port circulator can be analyzed as a one-port disk resonator with the single port subdivided. The summation terms in (15) are similar to those terms in (12) where s equal to l. The terms in (12) where the indices are equal correspond to the one-port disk resonator with that port segmented. The only difference between the one-port equation and the eigenvalue matrix in (15) is a factor of three in each term and the summation indices changed from n to $3v - k$.

The major savings in using the eigenvalue matrix expansion is in the number of operations required to invert the impedance matrices. For a circulator where each ports is subdivided into N subports, inverting the impedance matrix in (12) requires $27N^3$ products and $27N^3 - 18N^2 + 3N$ additions, while the inverting the three eigenvalue matrices requires only $3N^3$ multiplications and $3N^3 - 6N^2 + 3N$ additions. Table I shows the number of operations versus the number of subports per port. The index "1" denoted the number of numerical operations associated with inverting the impedance matrix generated with the direct approach. The "2" index corresponds to the number of operations required to invert three subport matrices. Even with as few as two subports, the number of operations required to invert the system is reduced very significantly.

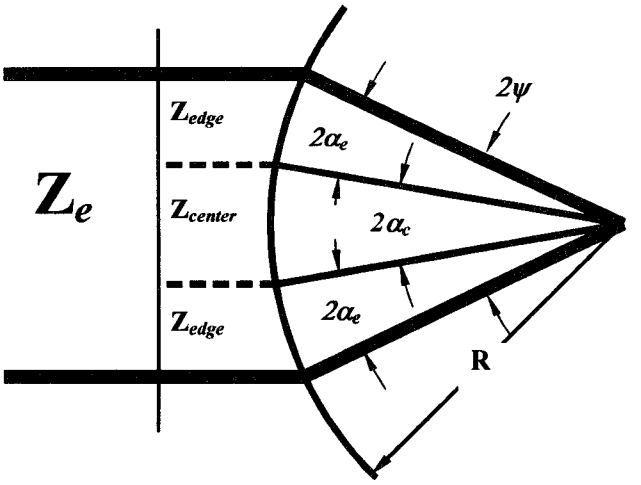

Fig. 4. Equivalent circuit of stripline feeding circulator with uneven subports.

IV. UNEQUAL SUBPORT WIDTH AND COUPLING ANGLE

The main limitation of Bosma's analysis is the unrealistic assumption of constant port current. The subport model improves agreement because the currents are allowed to vary across the strip. By using a lower outer subport impedance, the current distribution is allowed to follow the edge conditions. Therefore, a more accurate model results. A three-subport model is assumed, and we also assume that each subport is fed by an independent transmission line. This means that the outer subports have more current incident upon them than the inner subports. A constant voltage, V_e, across the entire strip is still assumed. The three independent transmission lines are now effectively in parallel until they enter the disk as shown in Fig. 4.

To reflect this stripline current density, we assume that the lead line width is less than $\lambda/4$. In this case, the current density just beyond the disk edge can be assumed to have the following tangential distribution [9], [11]:

$$J_s(\phi) = \frac{J_{s0}}{\sqrt{1 - \left(\frac{\phi}{\psi}\right)^2}} \quad (16)$$

where J_{s0} is the current at the center of the strip, ϕ is the location on the disk, and ψ is the coupling angle. This distribution is commonly found in literature [9], [11] for modeling stripline and microstrip lines. The total current is

TABLE II
NETWORK PARAMETERS—THREE-PORT CIRCULATOR

Network Parameter	Value
R : Disk Radius	0.225 inches
R_g: Garnet Radius	0.442 inches
$L_l = R_g - R$: Transformer Line Length	0.217 inches
w_l : Transformer Width	0.120 inches
$2\psi_t$: Total Coupling Angle	0.54 radians
H_{dc}:Applied DC Field	2500 Oe
$4\pi M_s$: Magnetization of Ferrite	1780 Ga
ε_f : Ferrite Dielectric Constant	14.5

found by simple integration over the strip width to be $J_{s0}\psi/2$. If the stripline impedance is assumed to be Z_e, then the stripline voltage is determined as $Z_e J_{s0}\psi/2$.

To determine the impedance of each line in Fig. 4, we model the stripline as three discrete transmission lines connected in parallel. The impedance of each line is evaluated by dividing the strip width into a center section and two edge sections. The current in each section is determined by integrating the current density over each section. The edge and center line impedance are found as the ratio of the stripline voltage and current in each section

$$Z_{edge} = \frac{2Z_e}{1 - \frac{2}{\pi}\,\mathrm{Sin}^{-1}(\Lambda)} \tag{17}$$

$$Z_{center} = \frac{Z_e}{\frac{2}{\pi}\,\mathrm{Sin}^{-1}(\Lambda)} \tag{18}$$

where Λ is the ratio of the central subport angle α_c to the total subport angle ψ. Based on the above current and impedance distribution, the eigenvalue matrix element equation (15) is modified to account for the unequal impedances and coupling angles

$$\{\mathbf{Z}_k\}_{lm} = j3Z_m\alpha_m \sum_{v=-\infty}^{\infty} M_{3v-k}(\alpha_l, \alpha_m)e^{-j(m-l)(3v-k)\vartheta} \tag{19}$$

where the subport stripline impedance Z_q, subport angle α_q, subport separation angle ϑ, and $M_n(x, y)$ are defined the following four equations:

$$Z_q = \begin{cases} Z_{edge} & q = 1, 3 \\ Z_{center} & q = 2 \end{cases} \tag{20}$$

$$\alpha_q = \begin{cases} \alpha_e & q = 1, 3 \\ \alpha_c & q = 2 \end{cases} \tag{21}$$

$$\vartheta = \alpha_c + \alpha_e \tag{22}$$

$$M_n(x, y) = \frac{\sin(nx)\sin(ny)}{n^2xy}\left[\frac{J_n'(\beta_e R)}{J_n(\beta_e R)} - \left|\frac{\kappa}{\mu}\right|\frac{n}{\beta_e R}\right]^{-1}. \tag{23}$$

Since we are assuming a lossless circulator, the matrix whose elements are determined in (19) must be normalized before the boundary conditions are applied so that we can determine the insertion loss, isolation, and impedance. The matrix whose elements are determined in (19) converts into a normalized skew-Hermitian matrix by applying (24) to the eigenvalue matrix $\mathbf{Z}_k$

$$\mathcal{Z}_k = Z_e\psi\mathbf{Z}_k\mathbf{Z}_{port}^{-1} \tag{24}$$

where $\mathbf{Z}_{port}$ is a diagonal matrix containing the subport impedances and coupling angles

$$\mathbf{Z}_{port} = \begin{bmatrix} Z_1\alpha_1 & 0 & 0 \\ 0 & Z_2\alpha_2 & 0 \\ 0 & 0 & Z_1\alpha_1 \end{bmatrix}. \tag{25}$$

The matrix $\mathcal{Z}_k$, whose elements are given in (26), are similar to the equal subport, equal impedance case

$$\{\mathcal{Z}_k\}_{lm} = j3Z_e\psi \sum_{v=-\infty}^{\infty} M_{3v-k}(\alpha_l, \alpha_m)e^{-j(m-l)(3v-k)\vartheta}. \tag{26}$$

If $\mathcal{Y}_k$ is the inverse of the skew symmetric matrix $\mathcal{Z}_k$, then the eigenvalues are found by (27)

$$y_k = \sum_{l=1}^{3}\sum_{m=1}^{3} \frac{Z_e\psi}{Z_m\alpha_m}\{\mathcal{Y}_k\}_{lm}. \tag{27}$$

V. EXPERIMENTAL RESULTS

The three-subport analysis of the three-post disk circulator was verified using a low microwave (1.5 GHz) circulator network shown in Fig. 1 using the dimensions in Table II. The circulator was made of 5-mil-thick brass, and it is sandwiched between two 0.884-inch-diameter ferrite disks to form a triplate stripline circulator with a total height of 0.085 ins. The ferrite material has a magnetization of 1780 Gauss, and the applied DC field was approximately 2500 Oersted. The internal field within the ferrite is assumed to be related to the DC magnetic field in the following manner:

$$H_{ferrite} = H_{dc} - 4\pi M_s. \tag{28}$$

The device was measured for isolation, insertion loss, and port impedance using an HP8753C network analyzer with an HP85044 Impedance Test Bridge.

The circulator was first simulated using equal-angle subports and equal subport stripline impedances. The network in Fig. 1 was placed between two circular ferrite disks in a triplate stripline structure as shown in Fig. 2. The circulator was modeled using 21 modes in the analysis. Each mode was assumed to be excited through a stripline which extends to the edge of the ferrite. The stripline length was approximately $\lambda/4$ long, and the frequency response of the feed line was included in the simulation. The above circulator was also modeled using different central subport angles with the subport impedances weighted accordingly. The number of modes was increased to 45 (−22 through +22) for the uneven impedance case since the narrower outer ports needed better resolution.

The frequency response of the isolation is shown in Fig. 5 and it is in fairly good agreement with the measured data. The isolator passband edges, defined as the 20-dB isolation frequencies, were located at 1.35 and 1.85 GHz. The two-subport

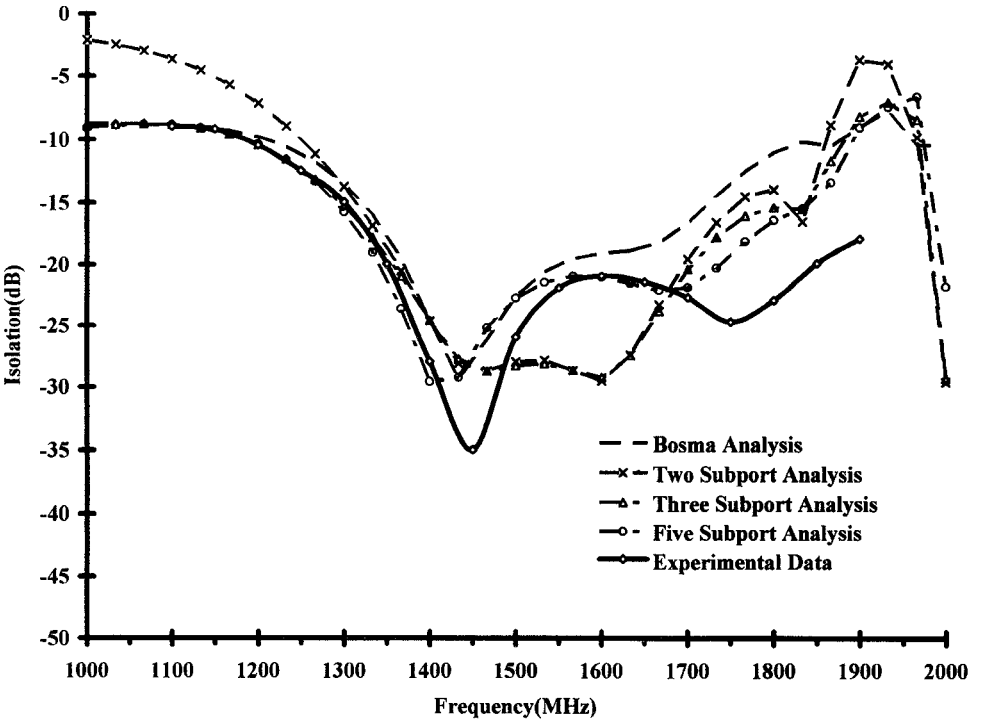

Fig. 5. Isolation versus frequency: equal-subport analysis, Bosma analysis, and experimental data.

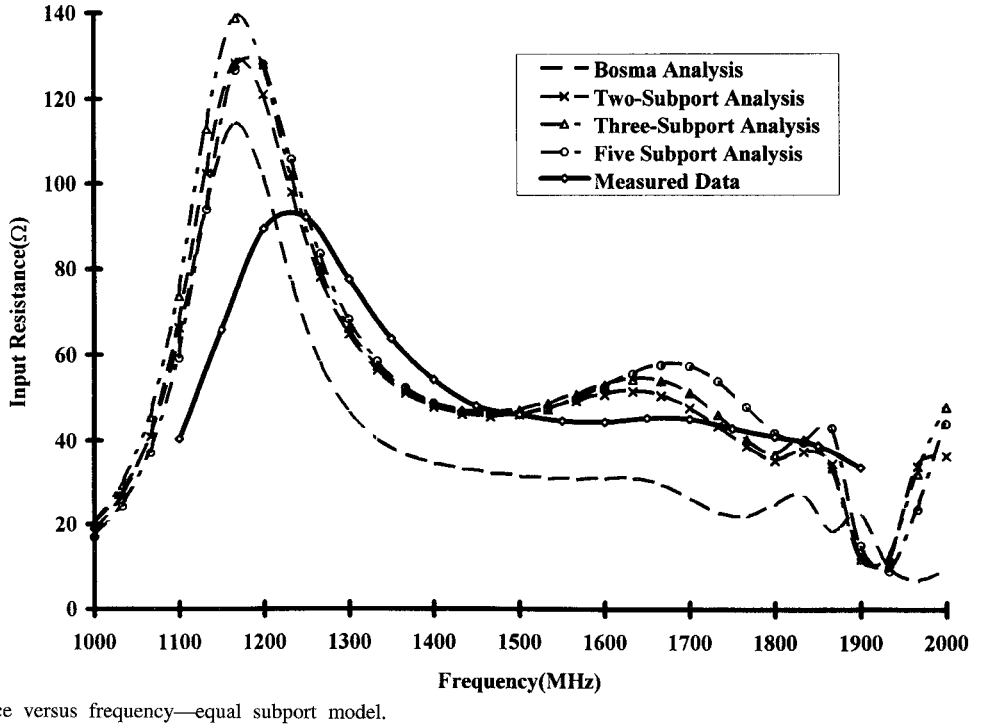

Fig. 6. Input resistance versus frequency—equal subport model.

analysis predicted these frequencies to be 1.34 and 1.71 GHz, while the three subport analysis predicts them to be 1.36 and 1.70 GHz. The five-subport model had the best agreement with 20-dB isolation frequencies of 1.34 and 1.72 GHz. The simulation based on Bosma's analysis predicts the 20 dB isolation frequencies to be 1.38 and 1.52 GHz.

The least isolation in the passband as determined from Fig. 5 is measured as 20.5 dB, and this isolation is located near the center of a double response. The five-subport results were the closest to measured results with the predicted isolation of 21 dB at the midband frequency. Bosma's analysis yielded only a single response with a predicted isolation of 29 dB in the center of the response.

Fig. 6 shows that the measured input impedance varies from 65 ohms to 40 ohms over the 1.35–1.85 GHz passband with an average value of 45 ohms. The predicted results using the subport analysis vary between 47.5 ohms for the two-subport case and 51.5 ohms for the five-subport case. The predicted

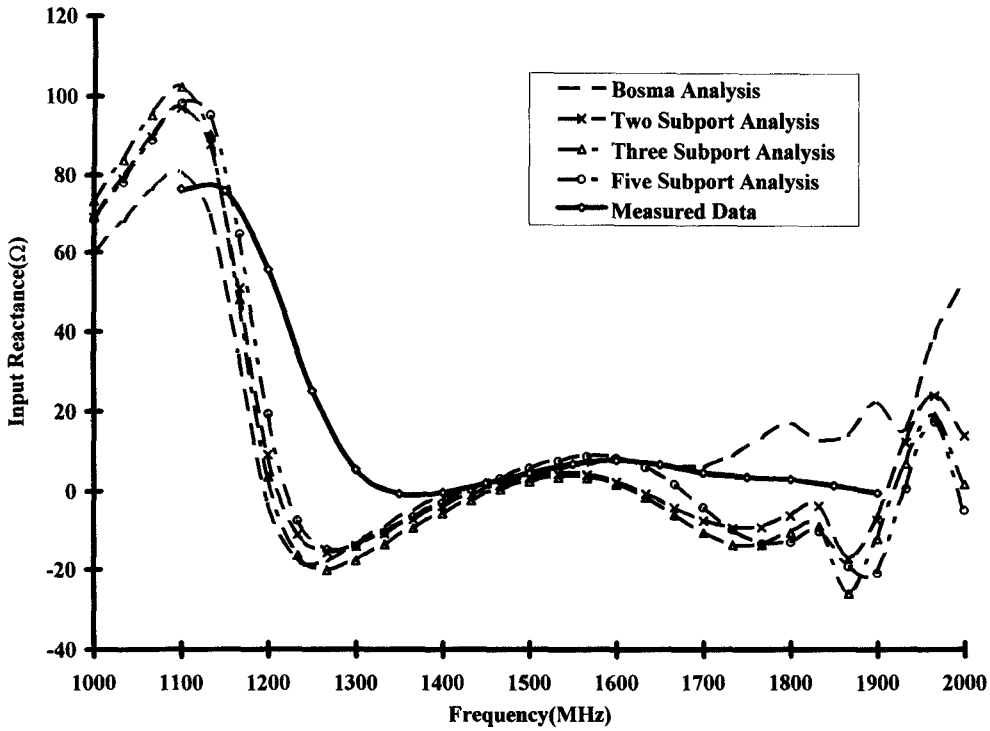

Fig. 7. Input reactance versus frequency—equal subport model.

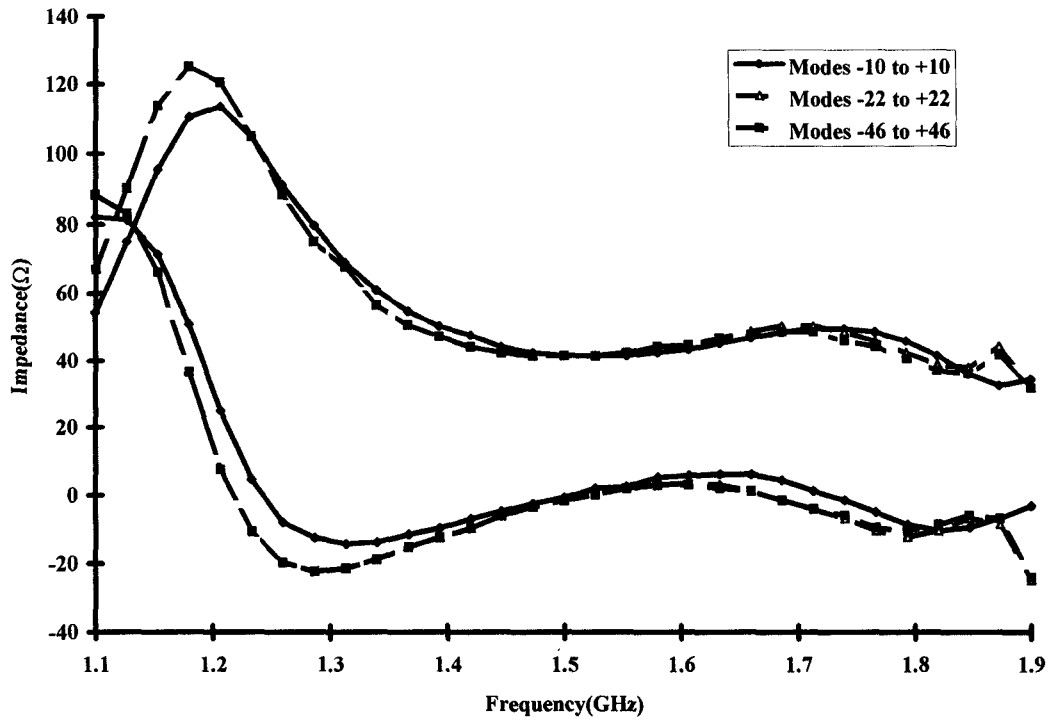

Fig. 8. Input impedance versus frequency—varying number of modes.

resistance using Bosma was 31.5 ohms, which is significantly lower than the measured data. The reactance response plotted in Fig. 7 shows that the predicted and measured results did not differ significantly. The resulting reactance was so small relative to the resistance that the reactance variation had little effect on the overall predicted performance. Overall, the three-subport segmentation seems to offer the best agreement with measured isolation and measured impedance.

In the above results, the summation range in (12) was taken to be from $-N$ to N, where N is the number of subports. This is equivalent to generating the direct subport matrix with summation indices ranging from $-(3N+1)$ to $3N+1$. The convergence of these results was studied versus the number of resonant modes. No advantage was observed in increasing the number of modes beyond the previously discussed limits. The weighting coefficients of the electric field at three frequencies

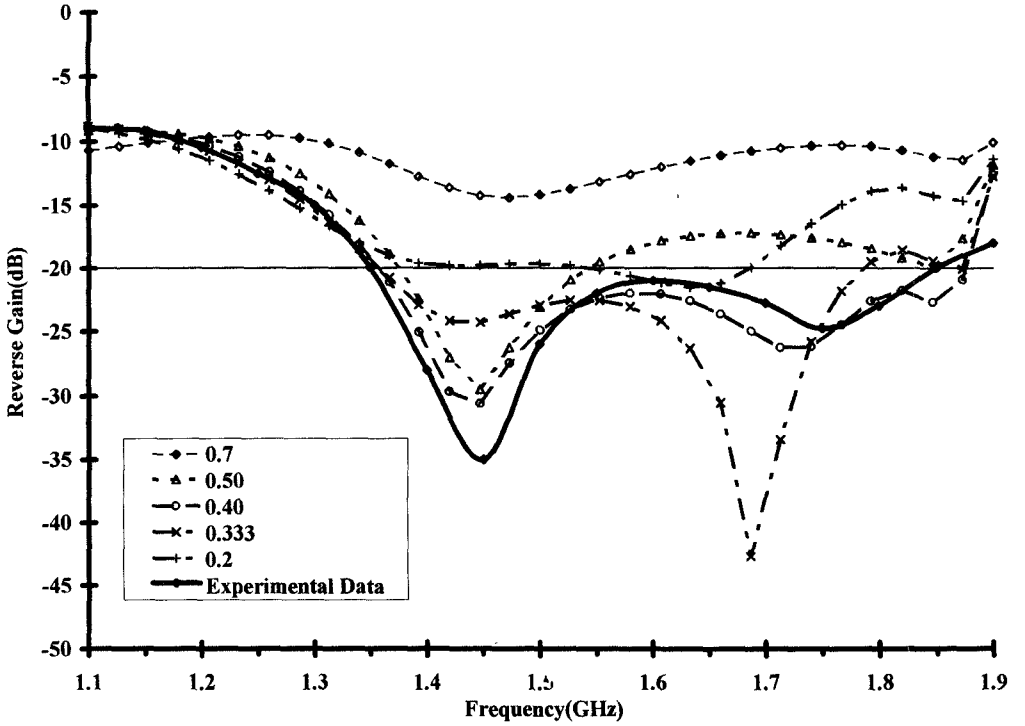

Fig. 9. Isolation versus frequency—uneven subport characteristics.

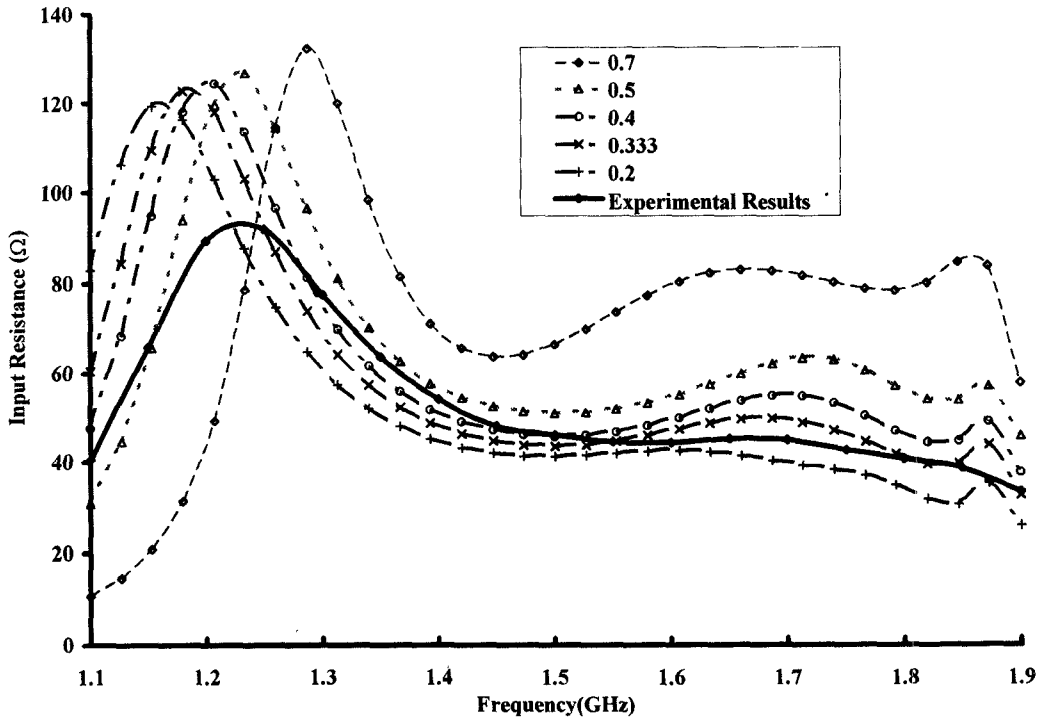

Fig. 10. Input resistance versus frequency—uneven subports.

in the circulator passband is shown in Table III for the three subport analysis. This table shows that most of the electric field in the disk is generated in the +1 through +5 modes. Most of the other modes are excited at a significantly lower level. Fig. 8 shows the convergence of the input impedance versus frequency curve for different summation ranges. Fig. 8 also confirms the convergence of the impedance for a small number of modes. The convergence of the isolation was even faster than the convergence of the impedance.

The effects of the unequal subport angles and impedances on isolation and impedance are presented in Figs. 7–9. Varying the subport angles, while keeping the subport impedances equal, is not physical (the subport impedance varies with the effective subport width). Therefore, changing of the subport

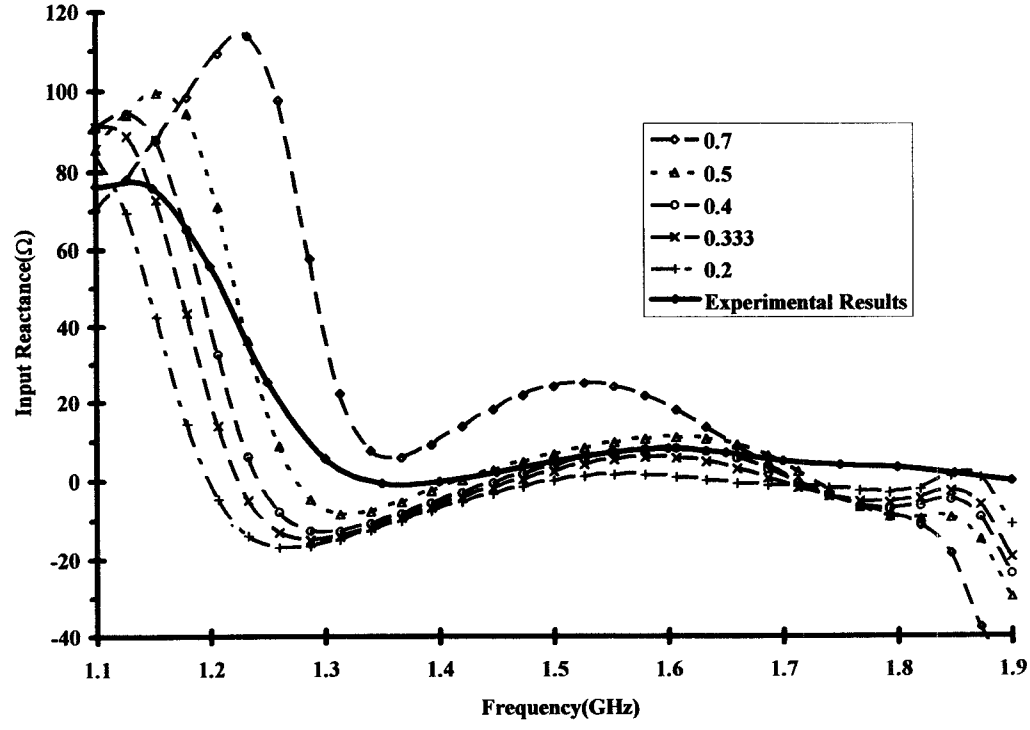

Fig. 11. Input reactance versus frequency—uneven subports.

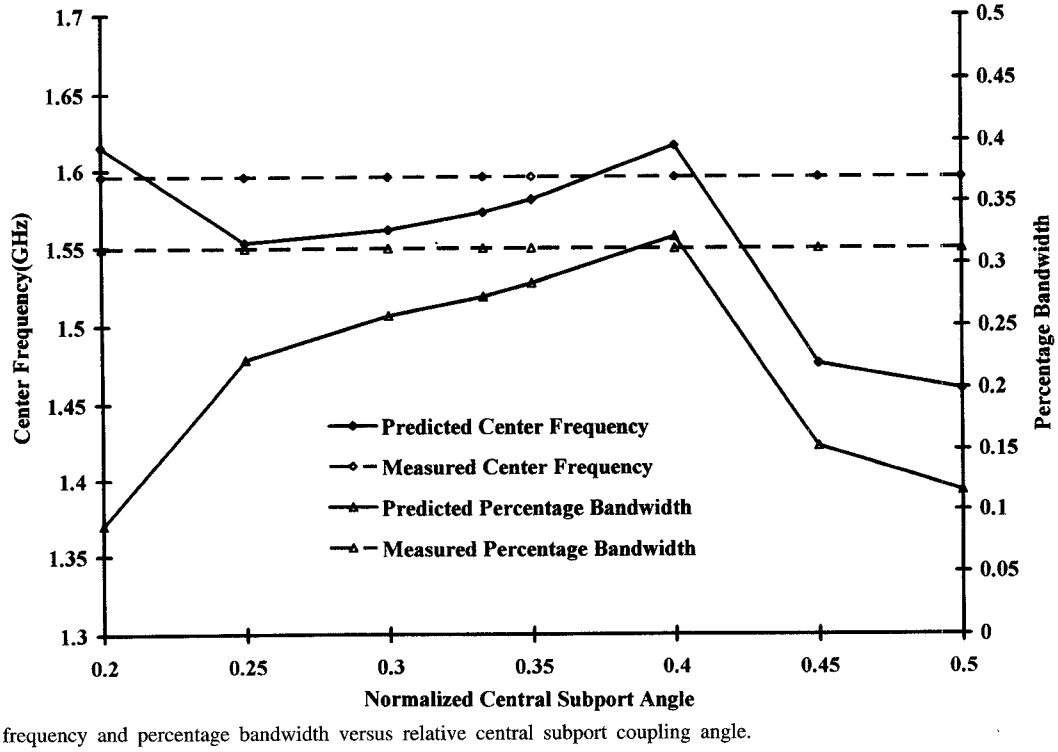

Fig. 12. Center frequency and percentage bandwidth versus relative central subport coupling angle.

impedances is coupled to the subport angles. The main input stripline impedance remains Z_e as in the equal subport angle and equal impedance case.

From Fig. 9, the isolation curve showed an improved agreement between the predicted results and the measured data over a range of subport angles. Between normalized central angles of 0.25 and 0.4, the variation was not particularly significant in terms of bandwidth and isolation. When the central angle fell below 0.25 or increased above 0.4, the discrepancy between the predicted and measured bandwidth and isolation increased.

Figs. 10 and 11 show that the predicted input impedance has good agreement with experimental data when the normalized central angle lies between 0.25and 0.5. Figs. 10 and 11 show that when the central angle is within that range, the input resistance at 1.6 GHz varies from 41 to 62 ohms, while the input reactance varies from -10 to $+10$ ohms. When the

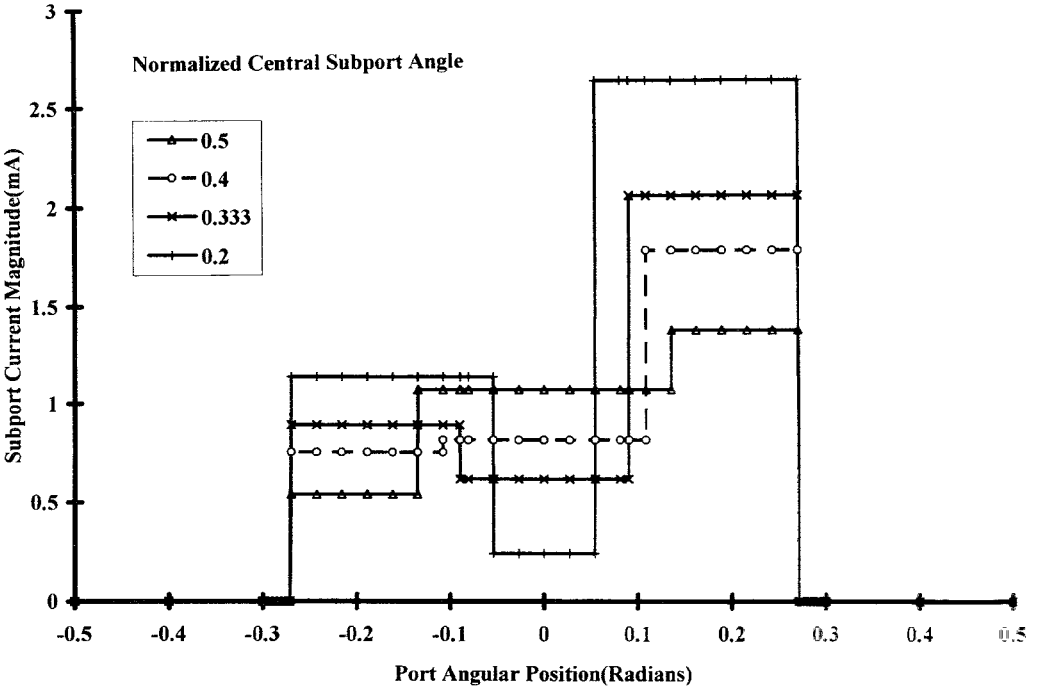

Fig. 13. Simulated input current distribution—varying central angle.

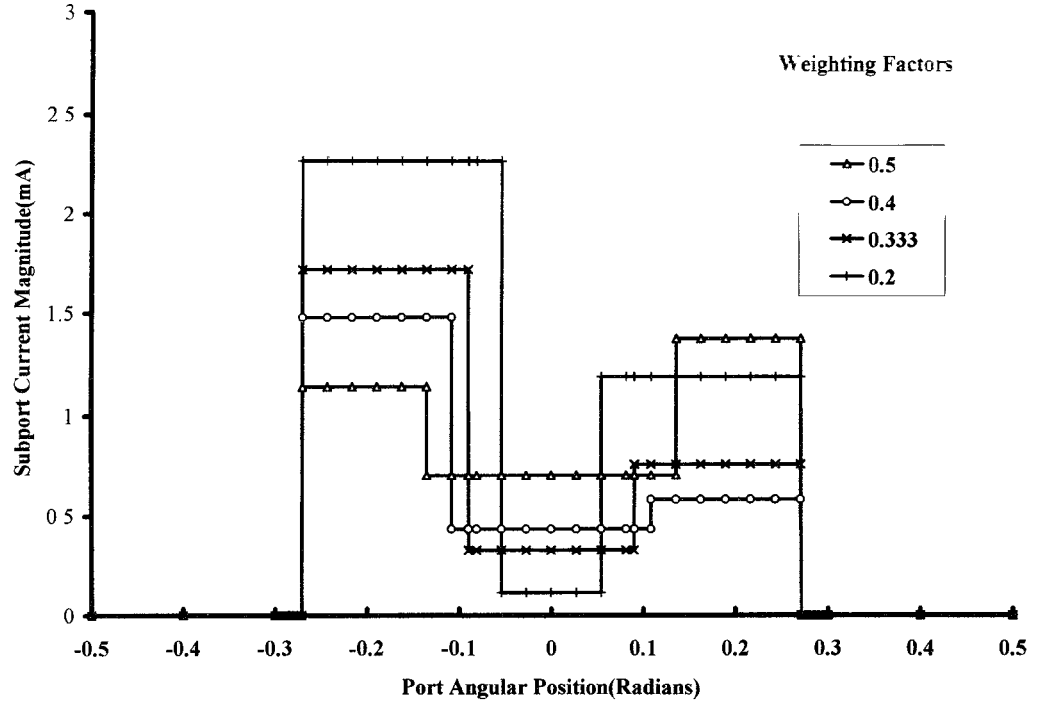

Fig. 14. Simulated output current distribution—varying central angle.

normalized central angle reaches 0.7, the resistance increases to 80 ohms and the reactance increases beyond 25 ohms. Also, as the central angle exceeds 0.5, the input impedance becomes unrealistic because at least one of the subports become too large to assume a constant current across it.

The center frequency and percentage bandwidth plotted versus normalized central angle in Fig. 12 shows that the analysis has fairly good agreement over the same range of relative central angles as those which accurately predicted the isolation frequency response and input impedance response. The center frequency varied between 1.56 and 1.62 GHz over a normalized central angle range of 0.25–0.40, while the experimental isolator had a center frequency of 1.56 GHz (an error of 1.2% error). The predicted bandwidth converged to 28% over most of the central angle range, while the measured results show a 31.2% bandwidth.

TABLE III
WEIGHTING OF ELECTRIC FIELD FOURIER SERIES TERMS

Mode	1.34 GHz	1.53 GHz	1.71 GHz
-4	0.0113	0.0006	0.0327
-3	0.0112	0.0006	0.0328
-2	0.0177	0.0010	0.0529
-1	0.0654	0.0039	0.2239
0	0.1064	0.0047	0.1764
+1	1.0000	1.0000	1.0000
+2	0.0609	0.0049	0.7320
+3	0.0825	0.0060	0.5607
+4	0.0720	0.0051	0.4307
+5	0.0088	0.0006	0.0499
+6	0.0302	0.0021	0.1664
+7	0.0339	0.0023	0.1840
+8	0.0239	0.0017	0.1286
+9	0.0094	0.0006	0.0502
+10	0.0134	0.0009	0.0709

Finally, in Figs. 13 and 14, the predicted current distribution of input and output port are presented for normalized central angles of 0.20, 0.333, 0.40, and 0.50. The current density is expected to be asymmetric due to the anisotropic behavior of the ferrite. [11] The predicted current in Fig. 13 reflects this tendency as it shows that the current on one edge is higher than that on the other due to ferrite nonreciprocity. In Fig. 14, the output current also shows the asymmetry and edge effects with the higher current on the opposite edge of the input port of the circulator.

From the results derived for the weighted subport analysis, the accuracy of the analysis seems to be good over a fairly wide range of subport angles, and the best accuracy seems to occur when the angles are closely equal. The improvement in accuracy using unequal subport impedances was noticeable for normalized central subport angles between 0.25 and 0.4. The only disadvantage was that the number of summation terms required for convergence was increased from $3N+1$ to roughly $4N$. Such an increase in the number of summation terms did not significantly reduce the numerical efficiency of the present approach.

VI. CONCLUSION

An accurate and numerically efficient analysis of a tightly coupled stripline junction circulator has been demonstrated. By calculating and solving for eigenvalue matrices instead of the overall impedance matrix, the number of operations decrease dramatically. The resulting equal-impedance subport analysis is shown to be accurate in center frequency, bandwidth, midband isolation, and optimum impedance for a tightly coupled circulator. Further accuracy improvement occurred by using uneven subport impedances to enhance the currents at the edge of the triplate stripline feeding the circulator. The weighted subport analyis required more summation modes, but the resulting accuracy improvement more than compensated for the slightly increased computing time.

REFERENCES

[1] H. Bosma, "On stripline circulator in UHF," *IEEE Trans. Microwave Theory Tech.*, vol. MTT-12, pp. 61–72, Jan. 1964.

[2] R. W. Lyon and J. Helszajn, "A finite element analysis of planar circulators using arbitrarily shaped resonator," *IEEE Trans. Microwave Theory Tech.*, vol. MTT-30, no. 11, pp. 1964–1974, July 1981.

[3] T. Miyoshi, S. Yamaguchi, and S. Goto, "Ferrite planar circuits in microwave integrated circuits," *IEEE Trans. Microwave Theory Tech.*, vol. MTT-25, no. 7, pp. 593–600, July 1977.

[4] T. Miyoshi and S. Miyauchi, "The design of planar circulators for wide-band operation," *IEEE Trans. Microwave Theory Tech.*, vol. MTT-28, no. 3, pp. 210–214, Mar. 1980.

[5] G. Riblet, "Techniques for broad-banding above-resonance circulators without the use of matching networks," *IEEE Trans. Microwave Theory Tech.*, vol. MTT-28, no. 2, pp. 125–129, Feb. 1980.

[6] K. Gaukel and E. El-Sharawy, "Three-port disk circulator analysis using only port segmentation," in *IEEE MTT-S Int. Microwave Symp. Dig.*, 1994, vol. 2, pp. 925–927.

[7] J. Helszajn and W. T. Nisbet, "Circulators using planar WYE resonators," *IEEE Trans. Microwave Theory Tech.*, vol. MTT-29, no. 7, pp. 689–699, Feb. 1980.

[8] J. Helozajn, *Non-Reciprocal Microwave Junctions and Circulators.* New York: Wiley, 1975, pp. 172–175.

[9] R. Mittra and C. Itoh, "Charge and potential distributions in shielded striplines," *IEEE Trans. Microwave Theory Tech.*, vol. MTT-18, pp. 149–156, 1970.

[10] C. Balanis, *Advanced Engineering Electromagnetics.* New York: Wiley, 1989, pp. 91–94.

[11] E. El-Sharawy and R. Jackson, "Rigorous analysis of infinitely long magnetostatic surface wave transducers," *IEEE Trans. Microwave Theory Tech.*, vol. 38, no. 6, pp. 730–738.

[12] T. Okoshi *et al.*, "The segmentation method—an approach to the analysis of microwave planar circuits," *IEEE Trans. Microwave Theory Tech.*, vol. MTT-24, pp. 662–668.

[13] G. Riblet and E. R. Hanson, "The use of symmetry to simplify the integral equation method with application to 6-sided circulator resonators," *IEEE Trans. Microwave Theory Tech.*, vol. MTT-30, no. 8, pp. 1219–1223.

[14] T. Okoshi and T. Miyoshi, "The planar circuit—An approach to microwave integrated circuitry," *IEEE Trans. Microwave Theory Tech.*, vol. MTT-20, no. 4, pp. 245–252, Apr. 1972.

Kevin M. Gaukel (M'94) received the B.S. degree from the University of Minnesota in 1983 and the M.S. degree from Arizona State University in 1994, both in electrical engineering.

From 1983–1985, he was a Receiver Design Engineer for E. F. Johnson in Waseca, MN. In 1986, he joined Celwave, R. F. in Phoenix, AZ as a Research and Development Engineer. He has developed broadband ferrite circulators and high-power coaxial resonators for 900 MHz and L-Band, and has assisted in the research of high-power waveguide and ceramic resonators. His research interests include high-power microwave components, numerical modeling of planar hybrid and ferrite networks, antennas, and complex phasing networks. He is cited in two patents involving high-power ceramic and coaxial resonators.

El-Badawy El-Sharawy (S'85–M'89–SM'92) received the B.Sc. and M.Sc. degrees (with honors) from Mansoura University, Eqypt, in 1980 and 1984, respectively, and the Ph.D. degree from the University of Massachusetts, Amherst, in 1989, all in electrical engineering.

He joined Arizona State University in 1989, where he is currently an Associate Professor of electrical engineering. His research interests are in the area of analysis and design of microwave circuits, anisotropic devices, and antennas.

Dr. El-Sharawy is a member of Eta Kappa Nu and Sigma Xi.